Oxidation of 5,15-Dioxaporphyrin: Its Generality and Novelty as an Oxaporphyrin Analogue

Hao, Jiping
Department of Applied Chemistry Graduate School of Engineering, Kyushu University

Nishiyama, Akihide
Department of Applied Chemistry Graduate School of Engineering, Kyushu University

Mori, Shigeki
Advanced Research Support Center (ADRES) Ehime University

Furukawa, Ko
Center for Coordination of Research Facilities Institute for Research Administrator Niigata University

他

出版情報：Angewandte Chemie International Edition. 62 (34), pp.e202307862-, 2023-08-17. Wiley
バージョン：

Oxidation of 5,15-Dioxaporphyrin: Its Generality and Novelty as an Oxaporphyrin Analogue

Jiping Hao,[a] Akihide Nishiyama,[a] Shigeki Mori,[b] Ko Furukawa,[c] and Soji Shimizu*[a]

[a] J. Hao, A. Nishiyama, Prof. Dr. S. Shimizu
Department of Applied Chemistry, Graduate School of Engineering and Center for Molecular Systems (CMS)
Kyushu University
Fukuoka 819-0395 (Japan)
E-mail: ssoji@cstf.kyushu-u.ac.jp

[b] Dr. S. Mori
Advanced Research Support Center (ADRES), Ehime University
Matsuyama 790-8577 (Japan)

[c] Prof. Dr. K. Furukawa
Center for Coordination of Research Facilities
Institute for Research Administrator, Niigata University
Niigata 950-2181 (Japan)

Supporting information for this article is given via a link at the end of the document.

Abstract: 5,15-Dioxaporphyrin (**DOP**) is a novel *meso*-oxaporphyrin analogue and exhibits unique 20π-antiaromaticity, unlike its mother congener of 18π-aromatic 5-oxaporphyrin, commonly known as its cationic iron complex called verdoheme as a key intermediate of the heme catabolism. To reveal reactivities and properties as an oxaporphyrin analogue, the oxidation reaction of tetra-β-arylated **DOP** (**DOP-Ar$_4$**) was explored in this study. Stepwise oxidation from the 20π-electron neutral state was achieved, and the corresponding 19π-electron radical cation and 18π-electron dication were characterized. Further oxidation of the 18π-aromatic dication resulted in the formation of a ring-opened dipyrrindione product via hydrolysis. Considering a similar reaction of verdoheme to ring-opened biliverdin in the heme degradation in nature, the current result consolidates the generality of ring-opening reactivity as an oxaporphyrinium cation species.

5-Oxaporphyrin, commonly known as its cationic iron complex called verdoheme,[1] has been an actively investigated heteroporphyrin analogue[2] to elucidate the enzymatic degradation mechanism of heme to biliverdin by heme oxygenases (Figure 1).[3] It is known that heme catabolism proceeds through three steps: (i) regiospecific hydroxylation at the *meso*-position of the porphyrin skeleton of heme to form *meso*-hydroxyheme; (ii) conversion of *meso*-hydroxyheme to verdoheme and removal of CO; and (iii) ring-opening of verdoheme to biliverdin and release of ferrous iron to maintain iron homeostasis.[4] Although the third step was reported to proceed by redox reactions using O_2 rather than hydrolysis, systematic studies on a variety of 5-oxaporphyrin metal complexes revealed the ring-opening reactivity of verdoheme derivatives toward nucleophiles as well as O_2 or H_2O_2 oxidant.[5,6] In contrast to the rich chemistry of 5-oxaporphyrin, other oxaporphyrin analogues have completely been unexplored until our synthesis of 5,15-dioxaporphyin nickel complex (**DOP**),[7] in which two opposite *meso*-carbon atoms in the porphyrin skeleton are replaced with oxygen atoms. Although our synthetic study of **DOP** was initiated by the interest in the creation of a stable antiaromatic compound based on the *meso*-heteroatom-modification strategy[2,8] to change the 18π-electron aromatic conjugated system of porphyrin to a 20π-electron antiaromatic one, we noticed the general reactivity of **DOP** as an oxaporphyrinium cation species[9] during the investigation on the oxidation reaction of **DOP**.

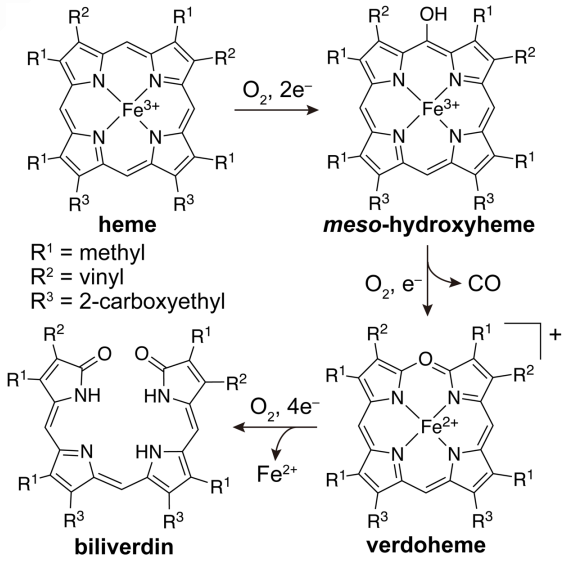

Figure 1. Verdoheme as a 5-oxaporphyrin derivative and heme degradation sequence catalyzed by heme oxygenases.

As with 5,15-diaminoporphyrin,[10,11] an isoelectric *meso*-nitrogen congener of **DOP**, **DOP** exhibits two reversible oxidation waves in the cyclic voltammogram, implying stepwise oxidation from the 20π-electron neutral state to a 19π-electron radical cation and further to an 18π-electron dication. However, chemical oxidation using silver(I) and nitrosonium oxidants provided β,β-linked dimer and tetrakis-β-nitrated **DOP**, respectively, as unexpected products, instead of the cationic species.[7,12] These results gave contrast to the oxidation of 5,10,15,20-tetraaryl-5,15-diaminoporphyrin, which provides stable 19π-electron radical cation and 18π-electron dication.[10] The electrochemical ESR measurements and spin density calculations of **DOP** revealed that the unique reactivities of **DOP** upon oxidation are ascribed to the high spin densities on the β-positions of the 19π-electron radical cation.

Herein, to prevent the side reactions and isolate oxidized species of **DOP** as stable forms, aryl groups were introduced to the β-positions of **DOP** by bromination and subsequent coupling reactions. Tetra-β-arylated **DOP** (**DOP-Ar$_4$**) synthesized in this context was successfully oxidized, and the corresponding cationic species were isolated and characterized. In addition, further oxidation of the 18π-electron dication using an excess amount of oxidant resulted in the formation of a ring-opened dipyrrindione due to a similar reactivity to verdoheme toward nucleophile, consolidating the generality of ring-opening reactivity as oxaporphyrinium cation species.

DOP-Ar$_4$ was synthesized from **DOP** by bromination with *N*-bromosuccinimide (NBS) and subsequent Suzuki-Miyaura coupling reaction with 4-methoxyphenylboronic acid (Scheme 1). The structure of **DOP-Ar$_4$** was unambiguously elucidated by high-resolution mass spectrometry, NMR spectroscopy, and single-crystal X-ray diffraction analysis (Figures 2, S1, S5, and S8 and Table S2).[13] As with the unsubstituted **DOP**,[7] **DOP-Ar$_4$** adopts a nearly planar structure with a small root-mean-square deviation (d_{RMS}) of 0.067 Å, indicating the minor steric effect of the 4-methoxyphenyl groups on the planar structure of **DOP**. Due to the weakly antiaromatic 20π-electron conjugated system, an upfield shift of the β-pyrrolic proton signal at δ = 5.82 ppm was observed in the ^{1}H NMR spectrum of **DOP-Ar$_4$** (Figure 3). Compared with the chemical shift of the β-pyrrolic proton of **DOP** at δ = 5.12 and 5.66 ppm, the slight downfield shift can be explained in terms of the local diatropic ring current effect of the neighboring 4-methoxyphenyl groups.

Oxidation of **DOP-Ar$_4$** was conducted using 2 equivalents of tris(4-bromophenyl)ammoniumyl hexachloroantimonate (Magic Blue), and the 18π-electron dication (**DOP-Ar$_4^{2+}$**) was obtained as a green solid (Scheme 2). The ^{1}H NMR spectrum of **DOP-Ar$_4^{2+}$** exhibits the downfield shift of the β-pyrrolic proton signal to δ = 8.03 ppm, indicating the conversion from the 20π-electron antiaromaticity of **DOP-Ar$_4$** to the 18π-electron aromaticity of **DOP-Ar$_4^{2+}$** (Figure 3) The nucleus-independent chemical-shift (NICS(0))[14] value at the midpoints designated in Figures 2 and 5 (**DOP-Ar$_4$**: δ = 4.13 and 4.45 ppm (***a***/***a'***) and δ = 5.54 and 5.71 ppm (***b***/***b'***) and **DOP-Ar$_4^{2+}$**: δ = –12.7 and –12.8 ppm (***a***/***a'***) and δ = –12.2 ppm (***b***/***b'***)) and anisotropy of the current-induced density (ACID)[15] plots calculated at the level of CAM-B3LYP/SDD for Ni and 6-311G(2d,p) for the rest of the atoms also support the antiaromaticity and aromaticity of the neutral and dication species, respectively (Figure S16 and Tables S6 and S7). As with the weak antiaromaticity of **DOP** and **DOP-Ar$_4$**, the downfield shift of the β-pyrrolic proton signal of **DOP-Ar$_4^{2+}$** is also modest compared with those of aromatic porphyrinoids. Considering that the β-pyrrolic proton signal of tetraoxaporphyrin dication reported by Vogel *et al.*,[16] which consists of four furan rings instead of pyrrole rings, was observed at δ = 11.17 ppm, it can be concluded that *meso*-oxygen atoms may lessen the global π-conjugation..

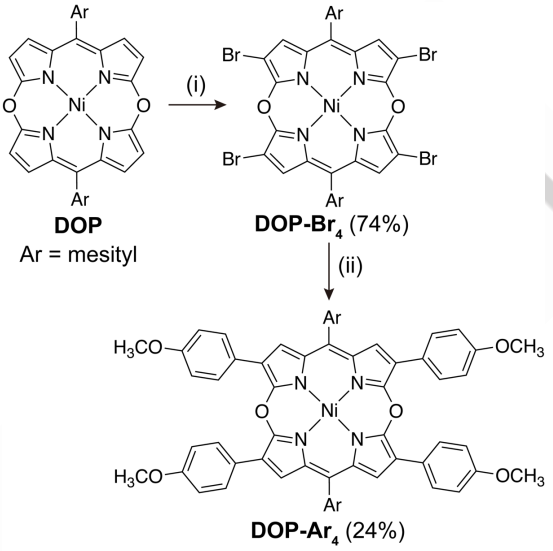

Scheme 1. Synthesis of **DOP-Ar$_4$**. Reagents and conditions. (i) NBS, THF, –78 °C, 1.5 h, then rt, 30 min. (ii) 4-methoxyphenylboronic acid, $Pd(OAc)_2$, K_2CO_3, cataCXium A, toluene, 100 °C, 24 h.

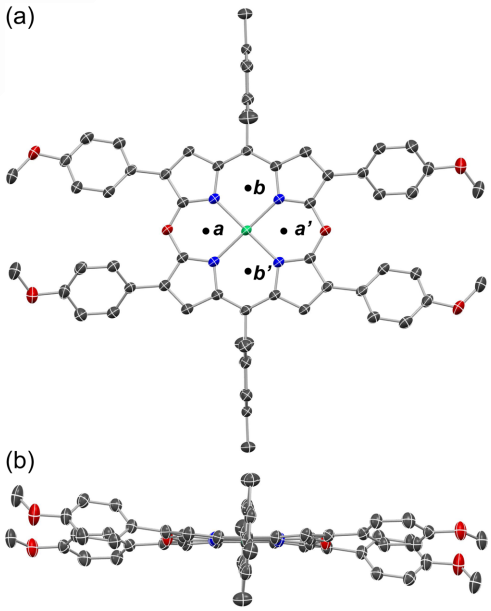

Figure 2. X-ray single-crystal structure of **DOP-Ar$_4$**, (a) top and (b) side views. The thermal ellipsoids are scaled to the 50% probability level. Hydrogen atoms are omitted for clarity. ***a***/***a'*** and ***b***/***b'*** in the top view denote the midpoints for the NICS(0) calculation.

Notably, **DOP-Ar$_4^{2+}$** is unstable in solution under ambient conditions and easily reduced to 19π-electron radical cation (**DOP-Ar$_4^{\bullet+}$**), which was confirmed by the disappearance of respective proton signals of **DOP-Ar$_4^{2+}$** in the ^{1}H NMR spectrum after an hour of storage in solution. The radical nature of **DOP-Ar$_4^{\bullet+}$** was characterized by the ESR spectrum (Figure S15). Therefore, a suitable single crystal of **DOP-Ar$_4^{2+}$** was grown under a nitrogen atmosphere in a glove box, whereas that of **DOP-Ar$_4^{\bullet+}$** was obtained on a benchtop under ambient conditions (Figures 4, 5, and S9–11 and Tables S3–5).[13] In the crystal structure of **DOP-Ar$_4^{2+}$**, two $SbCl_6^-$ counter anions reside above and below the molecular plane of **DOP-Ar$_4^{2+}$**, which is highly planar with d_{RMS} of 0.037 Å. The single crystals of **DOP-Ar$_4^{\bullet+}$** were grown by vapor diffusion of hexane or diethyl ether into a dichloromethane solution. In both cases, **DOP-Ar$_4^{\bullet+}$** molecules are arranged in a zig-zag manner, and one $SbCl_6^-$ counter anion is placed in the cleft formed by two **DOP-Ar$_4^{\bullet+}$** molecules. Compared with the neutral **DOP-Ar$_4$**, the C–O bond distance becomes shorter as the oxidation state increases: **DOP-Ar$_4$** (1.347–1.349 Å) > **DOP-Ar$_4^{\bullet+}$** (1.333–1.342 Å) > **DOP-Ar$_4^{2+}$** (1.332–1.334 Å), whereas the harmonic oscillator model of aromaticity (HOMA)[17] becomes closer to 1 (**DOP-Ar$_4$**: 0.659, **DOP-Ar$_4^{\bullet+}$**: 0.703 and 0.759, and **DOP-Ar$_4^{2+}$**: 0.714). These changes in the structure-based parameters reflect the conversion from antiaromaticity to aromaticity.

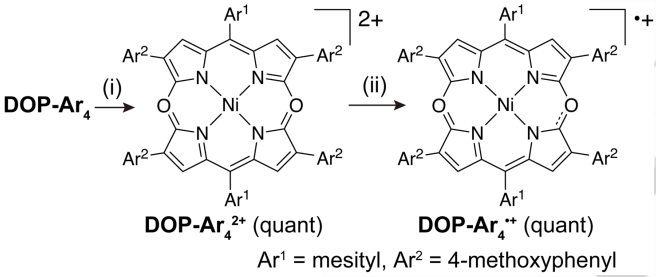

Scheme 2. Oxidation reaction of **DOP-Ar$_4$**. Reagents and conditions. (i) Magic Blue (2 eq), CH_2Cl_2, rt, 1 h. (ii) ambient conditions.

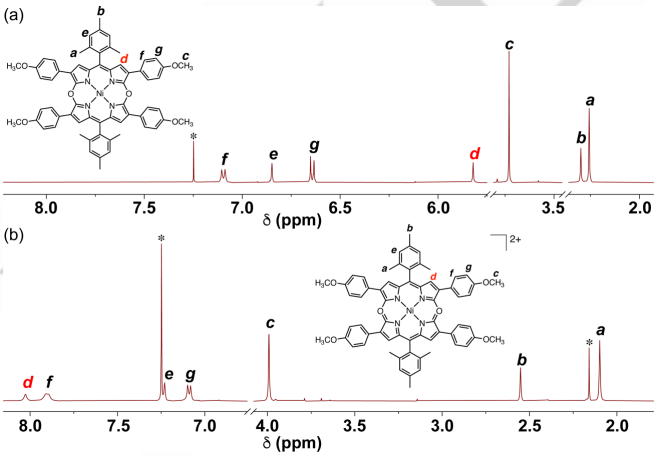

Figure 3. ^{1}H NMR spectra of (a) **DOP-Ar$_4$** and (b) **DOP-Ar$_4^{2+}$** in $CDCl_3$. Asterisks indicate residual solvent signals.

The absorption spectral changes upon oxidation were investigated by both chemical and electrochemical oxidations. The neutral **DOP-Ar$_4$** exhibits a similar absorption spectrum to that of unsubstituted **DOP** with a slight redshift of the main intense band at 534 nm by ca. 30 nm (Figure 6). A broad, ill-defined band ranging from 550 nm to 1000 nm is characteristic of an antiaromatic compound. Upon the addition of 1 equivalent of Magic Blue to a sample solution, an intense band with a vibronic shoulder arises at the absorption maximum wavelength (λ_{max}) of 1427 nm in the near-infrared (NIR) region. In the case of radical cation of 5,10,15,20-tetraaryl-5,15-diaminoporphyrin, a similar NIR band was also observed at λ_{max} = 860–890 nm and assigned as the characteristic optical properties of the 19π-electron radical cation species.[10a,b] Despite the significant redshift of the NIR band in our case, the observed spectral changes can sufficiently be ascribed to the formation of the 19π-electron radical cation species. Further addition of Magic Blue up to 2.5 equivalents caused attenuation of the NIR band, and a new broad band centered at 1030 nm arises. The overall absorption spectral profile was different from that expected for the porphyrin-like 18π-electron conjugated system, which comprises intense Soret and weak Q bands around 400 nm and 500–600 nm, respectively. Because of the accidental nondegeneracy of the LUMO orbitals, 18π-electron 5,15-diheteroporphyrin analogues exhibit rather intense Q band absorption with partially allowed nature according to Gouterman's four orbital theory for absorption properties of porphyrin and related macrocycles.[18] The isoelectric 18π-electron dication of 5,10,15,20-tetraaryl-5,15-diaminoporphyrin was reported to exhibit such a porphyrin-like absorption spectrum consisting of Soret and Q bands with similar intensities around 390 and 630 nm, respectively.[10a,b] In the electrochemical oxidation of **DOP-Ar$_4$**, similar absorption spectral changes were observed (Figures S13 and S14).

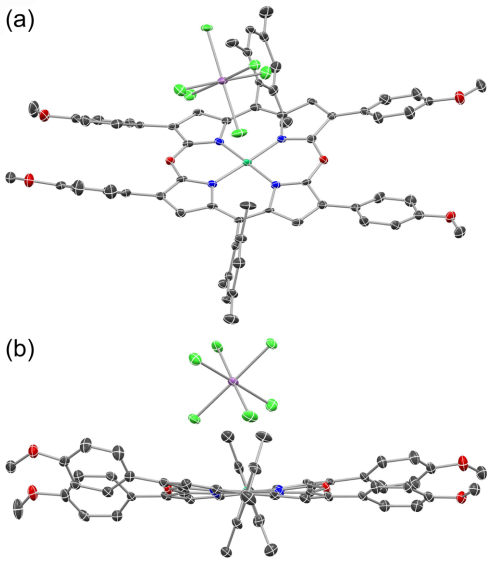

Figure 4. X-ray single-crystal structure of **DOP-Ar$_4^{\bullet+}$** (crystals were grown by vapor diffusion of hexane into a dichloromethane solution), (a) perspective and (b) side views. The thermal ellipsoids are scaled to the 50% probability level. Hydrogen atoms and a solvent molecule are omitted for clarity. The crystal structure of **DOP-Ar$_4^{\bullet+}$** grown in diethyl ether/dichloromethane is shown in Figure S10.

To give a detailed insight into the unique absorption spectrum of **DOP-Ar$_4^{2+}$**, the time-dependent (TD) DFT calculations were performed at the level of CAM-B3LYP/SDD for Ni and 6-31G(d) for the rest of the atoms (Figures S17–S22 and Tables S8–S12). The TDDFT calculations well reproduce the observed absorption spectral features for all the compounds, such as ill-defined broad absorption of **DOP-Ar$_4$** ranging from 550 to 1000 nm and intense

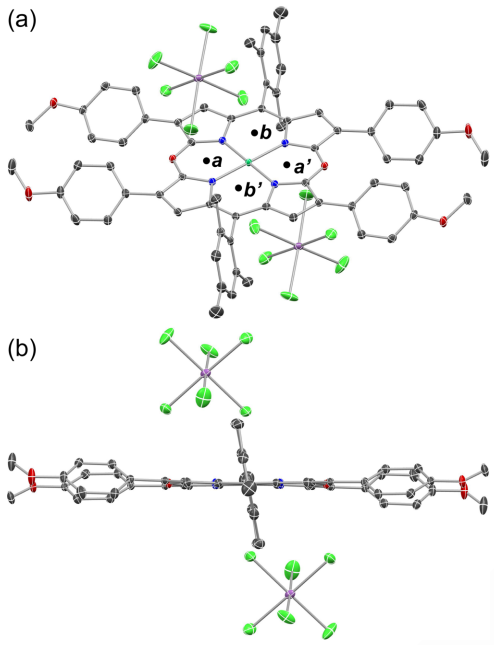

Figure 5. X-ray single-crystal structure of **DOP-Ar$_4^{2+}$**, (a) perspective and (b) side views. The thermal ellipsoids are scaled to the 50% probability level. Hydrogen atoms and a solvent molecule are omitted for clarity. ***a***/***a'*** and ***b***/***b'*** in the perspective view denote the midpoints for the NICS(0) calculation.

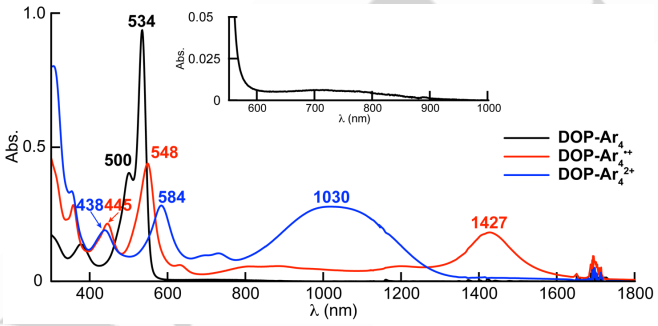

Figure 6. UV/vis/NIR absorption spectra of **DOP-Ar$_4$** (black line) and oxidized species (**DOP-Ar$_4^{\bullet+}$** (red line) and **DOP-Ar$_4^{2+}$** (blue line)) obtained by chemical oxidation with Magic Blue (1 eq for **DOP-Ar$_4^{\bullet+}$** and 2.5 eq for **DOP-Ar$_4^{2+}$**) in dichloromethane. The inset shows the absorption spectrum of **DOP-Ar$_4$** in the vis/NIR regions.

NIR band of **DOP-Ar$_4^{\bullet+}$** at 1429 nm.[19] As with porphyrin and 18π-electron 5,15-diheteroporphyrin analogues, the main theoretical absorption bands of **DOP-Ar$_4^{2+}$** consist of transitions between the four frontier orbitals, HOMO–1, HOMO, LUMO, and LUMO+1, which have the same number of nodal planes to those of the 18π-electron [16]annulene ($C_{16}H_{16}^{2-}$) parent hydrocarbon perimeter.[20] The calculated Q bands at 1124 and 931 nm mainly comprise HOMO→LUMO and HOMO–1→LUMO transitions, respectively, and show redshifts from those of a model dication structure without 4-methoxyphenyl groups (**DOP^{2+}**) calculated at the same level of theory. This can be explained by the molecular orbital (MO) interactions of the DOP core and the 4-methoxyphenyl groups, which more significantly destabilize the HOMO and HOMO–1 than the LUMO, narrowing the energy gaps. Therefore, the observed broad absorption of **DOP-Ar$_4^{2+}$** centered at 1030 nm can be assigned as two overlapped Q bands, and the unusual redshifts from Q bands of regular porphyrin and related analogues can be explained by the substituent effect.

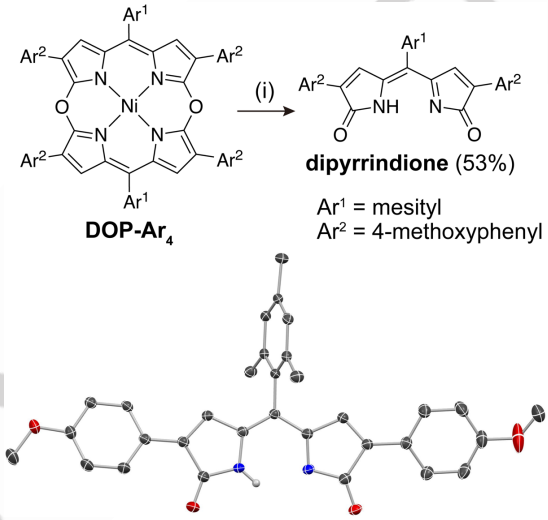

Scheme 3. Ring-opening reaction of **DOP-Ar$_4$** into dipyrrindione and its X-ray structure. Reagents and conditions. (i) Magic Blue (10 eq), CH_2Cl_2, rt, 1 h, then quenched with water.

During the chemical oxidation experiments, we found that when an excess amount of Magic Blue was used, ring-opened dipyrrindione was obtained instead of oxidized species (Scheme 3 and Figure S23). The structure was characterized by ^{1}H NMR spectroscopy and single-crystal X-ray diffraction analysis.[13] Oxidation with nitrosonium hexafluoroantimonate also provided the same product. Although reaction intermediates cannot be isolated and characterized, the close monitoring of the oxidation reaction revealed that the ring-opening reaction occurs when the reaction mixture is quenched with water. The maximum isolated yield of 53% indicates that a **DOP-Ar$_4$** molecule is converted into two dipyrrindione molecules. Taking these into consideration, the following plausible reaction mechanism can be proposed (Scheme S6). The initial step is the nucleophilic attack of water to the α-pyrrolic position next to the *meso*-oxygen atom with an oxonium ion nature at the dication state. The same reaction proceeds at the opposite position, breaking the tetrapyrrole into dipyrrin products. Demetallation also occurs at this step. Finally, the dipyrrin products bearing a hydroxy group(s) are oxidized to the dipyrrindione. This ring-opening reactivity is similar to that of verdoheme to biliverdin in the heme degradation sequence. Therefore, it can be concluded that upon oxidation, oxaporphyrin

analogues are prone to decompose into ring-opened products via nucleophilic substitution reaction due to the electron-withdrawing oxonium ion at the *meso*-positions.

In summary, the oxidized species of **DOP** were investigated using the tetra-β-arylated **DOP-Ar$_4$**, and the stepwise oxidation into the 19π-electron radical cation and the 18π-electron aromatic dication was achieved. In addition, the ring-opening reaction upon further oxidation in the presence of water was revealed as a common reactivity as oxaporphyrinium cation species, which have been exclusively seen in the heme degradation sequence from verdoheme to biliverdin. Considering that a ring-closing of biliverdin derivatives to 5-oxaporphyrins can be conducted in the reaction with an acid anhydride,[9] the obtained dipyrrindione can be a precursor for novel oxaporphyrin analogues, such as ring-expanded type compounds. Further investigations on the properties and reactivities of **DOP** can, therefore, enrich rather primitive oxaporphyrin chemistry, and research along this direction is intensively being pursued in our laboratory.

Acknowledgements

This work was supported by Grants-in-Aid from JSPS (No. JP22H02064), ENEOS Tonengeneral Research/Development Encouragement & Scholarship, and Toyota Riken Scholar from Toyota Physical and Chemical Research Institute.

Conflict of Interest

The authors declare no conflict of interest.

Data Availability Statement

The data that support the findings of this study are available in the supplementary material of this article.

Keywords: aromaticity • porphyrinoids • redox chemistry • radical • heme

[1] a) R. Schmid, A. McDonagh, in *The Porphyrins, Vol. VI* (Ed.: D. Dolphin), Academic Press, New York, **1978**; b) P. R. Ortiz de Montellano, *Curr. Opin. Chem. Biol.* **2000**, *4*, 221–227; c) P. R. Ortiz De Montellano, K. Auclair, in *The Porphyrin Handbook* (Eds.: K. M. Kadish, K. M. Smith, R. Guilard), Academic Press, Amsterdam, **2003**, pp. 183–210.

[2] Y. Matano, *Chem. Rev.* **2017**, *117*, 3138–3191.

[3] A. L. Balch, F. L. Bowles, L. P. Samankumara, in *Handbook of Porphyrin Science, Vol. 8*, World Scientific, Singapore, **2010**, pp. 293–342.

[4] T. Matsui, M. Unno, M. Ikeda-Saito, *Acc. Chem. Res.* **2010**, *43*, 240–247.

[5] a) A. L. Balch, L. Latos-Grażyński, B. C. Noll, M. M. Olmstead, L. Szterenberg, N. Safari, *J. Am. Chem. Soc.* **1993**, *115*, 1422–1429; b) A. L. Balch, M. Mazzanti, M. M. Olmstead, *J. Chem. Soc., Chem. Commun.* **1994**, 269–270; c) A. L. Balch, M. Mazzanti, T. N. St. Claire, M. M. Olmstead, *Inorg. Chem.* **1995**, *34*, 2194–2200; d) R. Koerner, L. Latos-Grażyński, A. L. Balch, *J. Am. Chem. Soc.* **1998**, *120*, 9246–9255; e) L. Latos-Grażyński, J. Johnson, S. Attar, M. M. Olmstead, A. L. Balch, *Inorg. Chem.* **1998**, *37*, 4493–4499; f) J. A. Johnson, M. M. Olmstead, A. L. Balch, *Inorg. Chem.* **1999**, *38*, 5379–5383; g) J. A. Johnson, M. M. Olmstead, A. M. Stolzenberg, A. L. Balch, *Inorg. Chem.* **2001**, *40*, 5585–5595; h) L. Latos-Grażyński, J. Wojaczyński, R. Koerner, J. J. Johnson, A. L. Balch, *Inorg. Chem.* **2001**, *40*, 4971–4977; i) K. T. Nguyen, S. P. Rath, L. Latos-Grażyński, M. M. Olmstead, A. L. Balch, *J. Am. Chem. Soc.* **2004**, *126*, 6210–6211.

[6] a) T. Yamauchi, T. Mizutani, K. Wada, S. Horii, H. Furukawa, S. Masaoka, H.-C. Chang, S. Kitagawa, *Chem. Commun.* **2005**, 1309–1311; b) R. Nakamura, K. Kakeya, N. Furuta, E. Muta, H. Nishisaka, T. Mizutani, *J. Org. Chem.* **2011**, *76*, 6108–6115; c) K. Kakeya, A. Nakagawa, T. Mizutani, Y. Hitomi, M. Kodera, *J. Org. Chem.* **2012**, *77*, 6510–6519.

[7] A. Nishiyama, M. Fukuda, S. Mori, K. Furukawa, H. Fliegl, H. Furuta, S. Shimizu, *Angew. Chem. Int. Ed.* **2018**, *57*, 9728–9733; *Angew. Chem.* **2018**, *130*, 9876–9881.

[8] S. Shimizu, *HETEROCYCLES* **2020**, *100*, 1123–1162.

[9] A. Takiguchi, S. Kang, N. Fukui, D. Kim, H. Shinokubo, *Angew. Chem. Int. Ed.* **2021**, *60*, 2915–2919; *Angew. Chem.* **2021**, *133*, 2951–2955.

[10] a) T. Satoh, M. Minoura, H. Nakano, K. Furukawa, Y. Matano, *Angew. Chem. Int. Ed.* **2016**, *55*, 2235–2238; *Angew. Chem.* **2016**, *128*, 2275–2278; b) K. Sudoh, T. Satoh, T. Amaya, K. Furukawa, M. Minoura, H. Nakano, Y. Matano, *Chem. Eur. J.* **2017**, *23*, 16364–16373; c) K. Sudoh, T. Hatakeyama, K. Furukawa, H. Nakano, Y. Matano, *J. Porphyrins Phthalocyanines* **2018**, *22*, 542–551.

[11] A. Yamaji, H. Tsurugi, Y. Miyake, K. Mashima, H. Shinokubo, *Chem. Eur. J.* **2016**, *22*, 3956–3961.

[12] A. Nishiyama, Y. Tanaka, S. Mori, H. Furuta, S. Shimizu, *J. Porphyrins Phthalocyanines* **2020**, *24*, 355–361.

[13] Deposition Numbers 2262487, 2262488, and 2262492–2262494 contain the supplementary crystallographic data for this paper. These data are provided free of charge by the joint Cambridge Crystallographic Data Centre and Fachinformationszentrum Karlsruhe Access Structures service www.ccdc.cam.ac.uk/structures.

[14] Z. Chen, C. S. Wannere, C. Corminboeuf, R. Puchta, P. v. R. Schleyer, *Chem. Rev.* **2005**, *105*, 3842–3888.

[15] a) D. Geuenich, K. Hess, F. Köhler, R. Herges, *Chem. Rev.* **2005**, *105*, 3758–3772; b) R. Herges, D. Geuenich, *J. Phys. Chem. A* **2001**, *105*, 3214–3220.

[16] a) E. Vogel, W. Haas, B. Knipp, J. Lex, H. Schmickler, *Angew. Chem. Int. Ed. Engl.* **1988**, *27*, 406–409; *Angew. Chem.* **1988**, *100*, 445–448; b) W. Haas, B. Knipp, M. Sicken, J. Lex, E. Vogel, *Angew. Chem. Int. Ed. Engl.* **1988**, *27*, 409–411; *Angew. Chem.* **1988**, *100*, 448–450.

[17] T. M. Krygowski, H. Szatylowicz, O. A. Stasyuk, J. Dominikowska, M. Palusiak, *Chem. Rev.* **2014**, *114*, 6383–6422.

[18] a) M. Gouterman, *J. Chem. Phys.* **1959**, *30*, 1139–1161; b) M. Gouterman, *J. Mol. Spectrosc.* **1961**, *6*, 138–163.

[19] The TDDFT calculations on **DOP-Ar$_4$** are described in detail in the Supporting Information.

[20] a) J. Michl, *J. Am. Chem. Soc.* **1978**, *100*, 6801–6811; b) J. Michl, *Tetrahedron* **1984**, *40*, 3845–3934; c) J. Michl, *Pure Appl. Chem.* **1980**, *52*, 1549–1563.

Entry for the Table of Contents

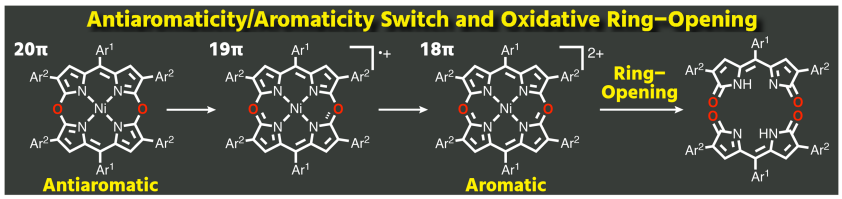

Conversion of 5,15-dioxaporphyrin from 20π-antiaromatic neutral state to 18π-aromatic dication state was achieved by blocking the reactive pyrrolic β-positions with aryl groups. The dication was further converted into dipyrrindione via a ring-opening reaction, which was observed for the first time except for the oxidation of verdoheme into biliverdin in the heme catabolism, consolidating a common reactivity as an oxaporphyrinium cation species.